Neuron, Volume *71*

Supplemental Information

Development of Cell Type-Specific Connectivity Patterns of Converging Excitatory Axons in the Retina

Joshua L. Morgan, Florentina Soto, Rachel O.L. Wong, and Daniel Kerschensteiner

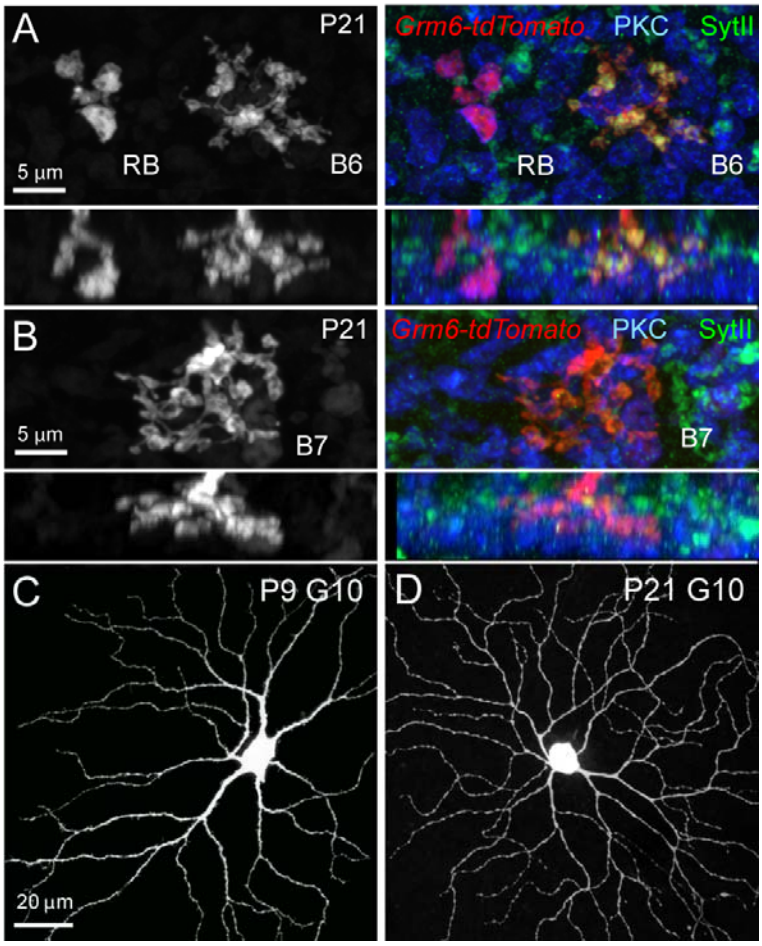

Figure S1 Cell Type-Specific Labeling of Neuron Pairs and Their Connections (Related to Figure 1)

(A - B) En face (*upper panels*) and orthogonal views (*lower panels*) of axons from isolated rod bipolar (RB), type 6 cone bipolar (B6), and type 7 cone bipolar (B7) cells labeled in retinal flat mounts from *Grm6-tdTomato* transgenic mice (*left panels*). Identification of these cell types was based on their characteristic morphology and confirmed by immunohistochemistry for PKCα and synaptotagmin2 (SytII) which labels RB and B6 cells, respectively (*right panels*). (C - D) G10 RGCs were labeled biolistically with cerulean fluorescent protein (CFP) and PSD95 fused to yellow fluorescent protein (PSD95-YFP, not shown in these panels). The cell type-specific dendritic morphology of G10 RGCs with primary branches (approximately six) that run relatively long before bifurcating into secondary processes of homogeneous caliber was easily identifiable at postnatal day 9 (P9, C) and P21 (D).

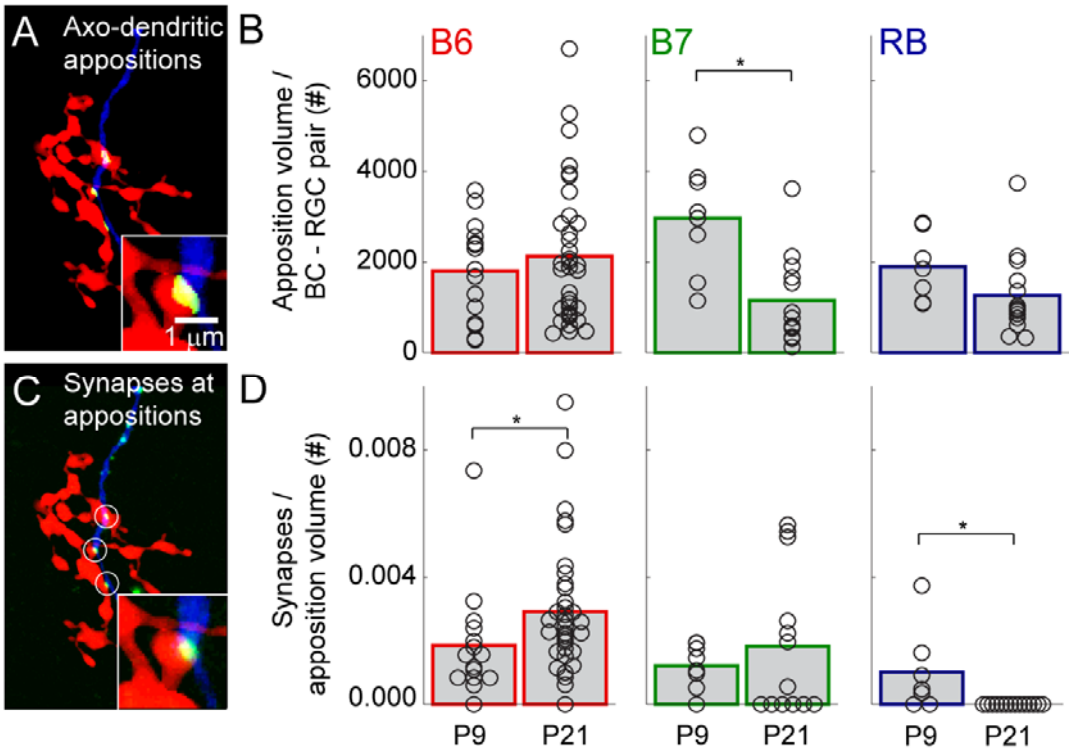

Figure S2 Changes in Synaptic Conversion but not Total Apposition Volume Determine Development of BC-RGC connectivity. (Related to Figure 2)

(A - B) Axo-dendritic appositions between BCs and RGCs were measured as the total number of overlapping voxels of B6 (B, *left*), B7 (B, *middle*) and RB (B, *right*) axons with G10 RGC dendrites at P9 and P21. Population data (B) show that changes in axo-dendritic overlap do not predict the divergent synaptic development of the different BC types with their shared target (s. Figure 2). (C - D) Instead changes in the number of synapses relative to the volume of axo-dendritic overlap accounts for the emergence of specific connectivity patterns between convergent B6 (D, *left*), B7 (D, *middle*) and RB (D, *right*) axons. These results are similar to those presented in Figure 3 and highlight that the observation of selective changes in the connectivity fraction holds independent of whether appositions are counted as discrete sites or measured by the total volume of axo-dendritic overlap. Throughout this figure each open circle represents average data from one cell pair, bars indicate the mean of the population and * signifies $p < 0.05$ (Wilcoxon-Mann-Whitney rank sum test).

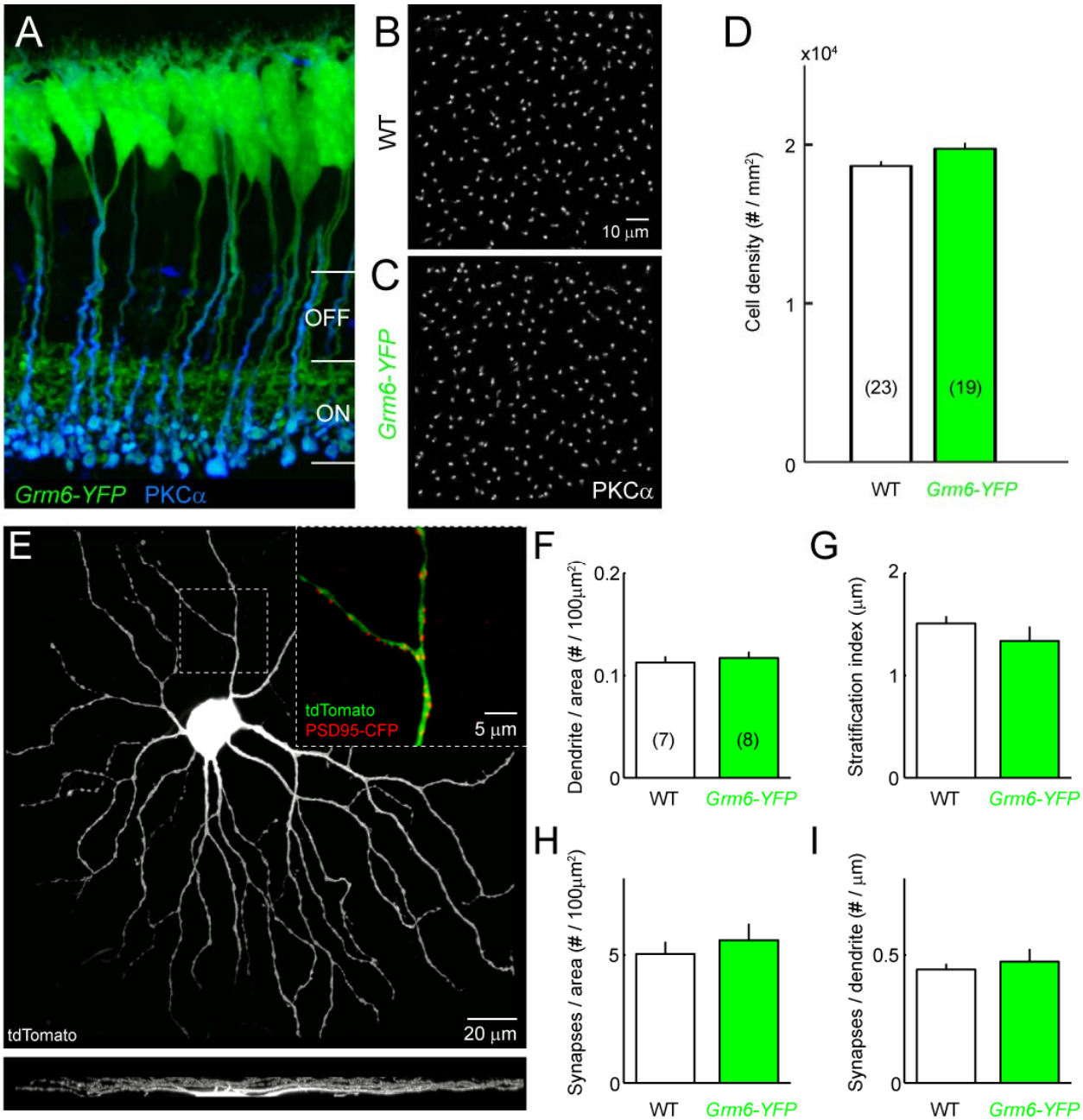

Figure S3 *Grm6-YFP* mice label most ON BCs, without changing cell density or the patterns of synapses between BCs and RGCs. (Related to Figure 3)

(A) Representative image of a vibratome section through the retina of a P21 *Grm6-YFP* mouse. BC terminals in the ON but not the OFF sublamina are densely labeled with YFP. Co-staining for PKCα demonstrates that all RBs in this section express YFP. In the *Grm6-YFP* transgene, YFP is followed by a transcription stop sequence. This YFP stop cassette is floxed and followed downstream by a sequence encoding an attenuated version of diphtheria toxin (Breitman et al.,

1990). (B - D) To verify that in the absence of Cre recombinase cell viability was unchanged we compared the density of RBs between wildtype and *Grm6-YFP* retinas by counting the number of axon stalks in optical sections of flat mount preparations stained with anti-PKCα. The number of retinas that were assessed this way is indicated in brackets in the bar plots in D. (E) To test whether BCs formed normal patterns of synapses on RGC dendrites, we biolistically labeled RGCs in P21 *Grm6-YFP* mice and wildtype littermates with tdTomato and PSD95-CFP. (F - I) Population data show that the lateral branching (F) and stratification (G) of RGC dendrites, as well as the linear (H) and areal (I) density of BC synapses formed onto them were indistinguishable between wildtype and *Grm6-YFP* mice. The number of RGCs reconstructed in this analysis is denoted in the bar plots in (F). Bars (error bars) throughout the figure represent mean (±SEM) of the respective data sets.

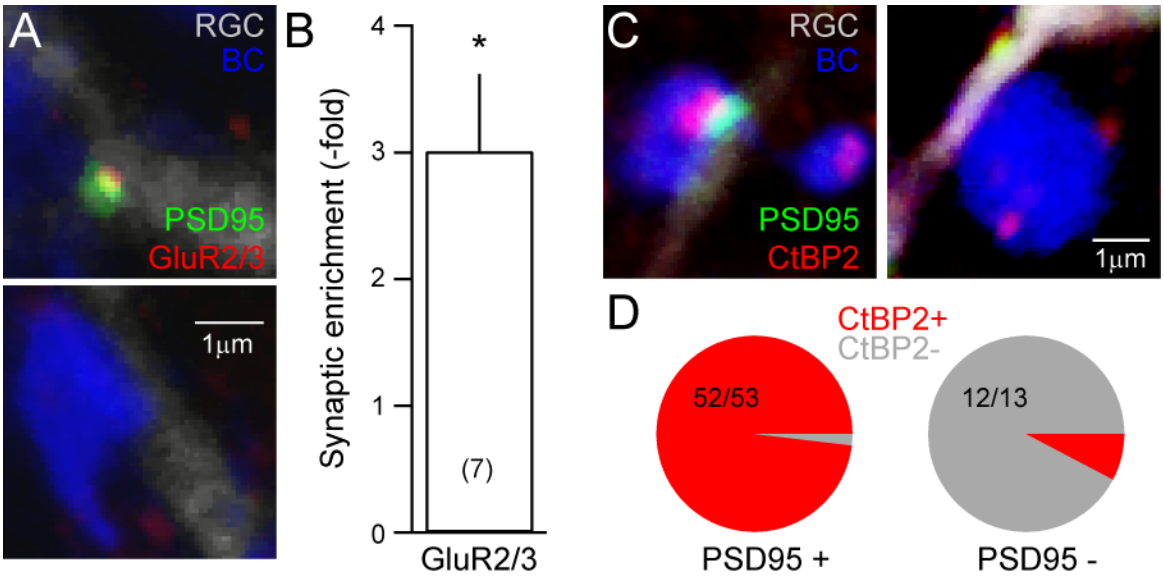

Figure S4 Axo-Dendritic Appositions with PSD95 are Enriched in Glutamate Receptors and Contain Presynaptic Release Sites More Frequently than Appositions without PSD95. (Related to Figure 4)

(A - B) Representative images (A) and summary data (B, mean ±SEM) showing that glutamate receptors accumulate at PSD95-positive appositions of BC axons and RGC dendrites at P9. We previously showed that glutamate receptors cluster at newly formed synapses between BCs and RGCs (Kerschensteiner et al., 2009). Here, we tested explicitly whether glutamate receptors are enriched at appositions containing PSD95 clusters compared to other areas of axo-dendritic contact. Towards this end, we biolistically labeled G10 RGCs in *Grm6-YFP* mice with tdTomato and PSD95-CFP. Retinas were then fixed and stained with an antibody against glutamate receptor subunits 2 and 3 (GluR2/3). An independent threshold was applied to the YFP (BC) and tdTomato (RGC) signals to binarize the respective images and identify areas of overlap (i.e. the product of the binarized images). PSD95-CFP clusters were identified automatically using an algorithm described before (Kerschensteiner et al., 2009; Morgan et al., 2008). We then calculated the ratio of the average GluR2/3 signal at synapses of one RGC and the average signal of all non-synaptic voxels of its appositions with BC axons after subtracting from each the average signal within the dendrite for normalization. A similar algorithm was used before to analyze activity-dependent changes in the synaptic accumulation of glutamate receptors (Lee et al., 2010). (C) Representative images of axo-dendritic appositions with (*left panel*) and without PSD95 clusters (*right panel*) in *Grm6-tdTomato* mice. RGCs and their synapses with BCs were labeled biolistically with CFP and PSD95-YFP, respectively. Presynaptic release sites were

simultaneously visualized using an antibody against CtBP2. (D) Population data showing that ~98 % (52 / 53) of appositions with PSD95 clusters also held CtBP2 puncta, whereas ~92 % (12 / 13) of appositions without PSD95 did not. Because presynaptic ribbons are not yet present at P9 (Johnson et al., 2003), these experiments were performed at P21. Together, the results presented in this figure support the classification of PSD95-containing appositions as synaptic and of appositions lacking PSD95 as non-synaptic.

Supplemental Experimental Procedures

Transgenic Mice

In the *Grm6-YFP* transgenic construct, the sequence encoding YFP and an ensuing transcription stop signal are flanked by loxP sites and an attenuated version of diphtheria toxin follows the second loxP site. We verified that in the absence of Cre recombinase only YFP is expressed and that BC numbers and synaptogenesis are unaffected in *Grm6-YFP* mice (Figure S2).

Image Processing and Analysis

To classify RGCs, image stacks from retinal flat mount preparations were acquired with sufficient field of view to include the entire RGC dendritic arbor. In addition to fluorescence from RGCs and BCs we collected reflected laser light to visualize the borders of the IPL. RGCs were classified based on stratification depth and lateral branching patterns as in several previous studies. Briefly, G10 RGCs (Volgyi et al., 2009) - equivalent to type C2i (Sun et al., 2002), cluster 9 (Badea and Nathans, 2004), cluster 11 (Kong et al., 2005), and type M10 (Coombs et al., 2006) - have large somata (~20 μm), 5 - 6 long primary dendrites and sparse branching patterns. Moreover, their dendrites stratify at the border of sublaminae S4 and S5 of the IPL and overlap with the axons of B6, B7 and RB BCs.

Similarly, BC types can be identified based on their morphology (Ghosh et al., 2004). In *Grm6-tdTomato* mice, brightly fluorescent cells mostly belong to one of three types. Narrow BC axon arbors forming few large terminal boutons in S5 with little or no branching outside of S5 were classified as belonging to RB cells. B7 cells were identified by axons branching almost exclusively in S4 and extending processes strictly parallel to the borders of the IPL. While axons of B6 cells also arborize mostly in S4, they could be distinguished from B7 cells by their more diffuse stratification which resulted in a significant number of terminals being found in S5. Finally, we confirmed our morphological identification of these BC types by staining flat mounts with anit-PKCα and anti-synaptotagmin 2 antibodies which label RB and B6 BCs, respectively (Fox and Sanes, 2007; Masu et al., 1995). This confirmed the cell type assignments made based on morphology.

Appositions between BCs and RGCs were identified by creating binary masks of each cell in Amira. Each binary mask was the result of an isointensity threshold and was manually edited to make sure that it did not bleed into the processes of nearby cells. BC and RGC masks were then smoothed in Matlab in order to expand the surfaces by a voxel and to prevent surface

irregularities from generating extra apposition sites. Appositions were defined as sites where a BC mask and an RGC mask overlapped by more than 50 connected voxels. We verified that appositions identified in this manner matched those identified by eye in > 90% of the cases. In addition, we made sure that our conclusions did not change when varying the voxel-threshold for appositions or when we measured the overall overlap of axonal and dendritic masks rather than determine the number of appositions (Figure S2).

To measure the overall number and density of BC synapses on G10 RGCs, we acquired confocal image stacks encompassing RGC dendrites completely at a voxel size of: 0.103 - 0.103 - 0.3 μm (*x-y-z*) from cells biolistically labeled with CFP and PSD95-YFP (for comparison of P9 and P21) or tdTomato and PSD95-CFP (for comparison of wildtype and *Grm6-YFP* mice). We then skeletonized dendrites and identified synaptic puncta using previously described algorithms (Kerschensteiner et al., 2009; Morgan et al., 2008).

Supplemental References

Badea, T.C., and Nathans, J. (2004). Quantitative analysis of neuronal morphologies in the mouse retina visualized by using a genetically directed reporter. J Comp Neurol *480*, 331-351.

Breitman, M.L., Rombola, H., Maxwell, I.H., Klintworth, G.K., and Bernstein, A. (1990). Genetic ablation in transgenic mice with an attenuated diphtheria toxin A gene. Mol Cell Biol *10*, 474-479.

Coombs, J., van der List, D., Wang, G.Y., and Chalupa, L.M. (2006). Morphological properties of mouse retinal ganglion cells. Neuroscience *140*, 123-136.

Fox, M.A., and Sanes, J.R. (2007). Synaptotagmin I and II are present in distinct subsets of central synapses. J Comp Neurol *503*, 280-296.

Ghosh, K.K., Bujan, S., Haverkamp, S., Feigenspan, A., and Wassle, H. (2004). Types of bipolar cells in the mouse retina. J Comp Neurol *469*, 70-82.

Johnson, J., Tian, N., Caywood, M.S., Reimer, R.J., Edwards, R.H., and Copenhagen, D.R. (2003). Vesicular neurotransmitter transporter expression in developing postnatal rodent retina: GABA and glycine precede glutamate. J Neurosci *23*, 518-529.

Kerschensteiner, D., Morgan, J.L., Parker, E.D., Lewis, R.M., and Wong, R.O. (2009). Neurotransmission selectively regulates synapse formation in parallel circuits in vivo. Nature *460*, 1016-1020.

Kong, J.H., Fish, D.R., Rockhill, R.L., and Masland, R.H. (2005). Diversity of ganglion cells in the mouse retina: unsupervised morphological classification and its limits. J Comp Neurol *489*, 293-310.

Lee, M.C., Yasuda, R., and Ehlers, M.D. (2010). Metaplasticity at single glutamatergic synapses. Neuron *66*, 859-870.

Masu, M., Iwakabe, H., Tagawa, Y., Miyoshi, T., Yamashita, M., Fukuda, Y., Sasaki, H., Hiroi, K., Nakamura, Y., Shigemoto, R., and et al. (1995). Specific deficit of the ON response in visual transmission by targeted disruption of the mGluR6 gene. Cell *80*, 757-765.

Morgan, J.L., Schubert, T., and Wong, R.O. (2008). Developmental patterning of glutamatergic synapses onto retinal ganglion cells. Neural Dev *3*, 8.

Sun, W., Li, N., and He, S. (2002). Large-scale morphological survey of mouse retinal ganglion cells. J Comp Neurol *451*, 115-126.

Volgyi, B., Chheda, S., and Bloomfield, S.A. (2009). Tracer coupling patterns of the ganglion cell subtypes in the mouse retina. J Comp Neurol *512*, 664-687.